Journal of Electronic Materials (2024) 53:5184–5192
https://doi.org/10.1007/s11664-024-11212-8

28TH INTERNATIONAL CONFERENCE ON NUCLEAR TRACKS AND RADIATION MEASUREMENTS

Structural, Optical, and Electrical Properties of FMWCNTs/CuS Nanocomposites

Yukti Gupta[1] · Mayank Mittal[1] · Manoj Giri[2] · Neena Jaggi[1]

Received: 15 December 2023 / Accepted: 23 May 2024 / Published online: 12 June 2024

Abstract
Carbon nanotube-based nanocomposites are most encouraging materials in the field of gas sensing. The nanocomposites with transition metals boost various properties of functionalized multiwalled carbon nanotubes (FMWCNTs), thus making them more appropriate for sensing applications. In this work, copper sulfide (CuS) nanoparticles prepared via a hydrothermal route were mixed with FMWCNTs by using a facile sonication method. The effect of CuS content in FMWCNTs/CuS nanocomposites was investigated using various characterization techniques. X-ray diffraction elucidated the formation of CuS nanoparticles along with the decrease in crystallite size of the nanocomposite. The optical behavior of the synthesized nanocomposite was studied using photoluminescence spectroscopy, which revealed an increase in the lifetime of the nanocomposite with the increase in CuS content. The absorption analysis shows an increase in the value of the bandgap with an increase in wt% of CuS in the nanocomposites. Electrical studies examined by *I–V* analysis confirmed the conducting nature of all three samples. The results reveal that FWMCNTs/CuS could be a potential material for sensing applications.

Keywords FMWCNTs · covellite CuS · bandgap · Raman analysis · electrical conductivity

Introduction

Metal chalcogenides have attracted many researchers and scientists due to their attractive optical and electrical properties, and their nanocomposites with other carbon-based materials are the latest topic of research. This trend is due to the enhancements observed in the properties of nanoparticles which are useful in various applications such as gas sensing, supercapacitors, sensors, etc.[1–4] Nanocomposites, which include nanostructured transition metal sulfides, such as CdS, ZnS, PbS, HgS, and CuS,[5–7] have distinctive chemical and physical properties compared to their bulk phases. They have low cost, a variety of morphologies, high specific surface areas, and the ability to promote electron transfer reactions.

Different research groups have performed various applications based on nanocomposites of carbon-based materials with metal chalcogenide nanoparticles. Goswami et al. studied a PANI/MWCNTs-ZnS composite and stated that incorporation of ZnS in PANI/MWCNTs leads to a 23.1% enhancement in the magneto-conductivity of MWCNTs, which validates them as a potential candidate for the electronic industry.[8] Sahu et al. have successfully synthesized MWCNT nanocomposites with ZnS and CdS which were demonstrated to degrade methylene blue dye. They revealed that MWCNTs/CdS nanocomposites show better degradation efficiency compared to MWCNTs/ZnS.[9] Taleb et al. reported the synthesis of CuS, CuS/CNTs, and CuS/CNTs/gCN through a hydrothermal method, which revealed CuS/CNTs/gCN to be a potential nanomaterial to compete in water pollution for remediation of both cationic and anionic contaminants.[10] Zhang et al. hydrothermally synthesized CuS nanoparticles and CuS/rGO nanocomposites. They explored the photocatalytic performance of methylene blue dye to enhance photocurrent generation in visible light in CuS/rGO nanocomposites compared to pure CuS nanoparticles.[11] Sabeeh et al. studied the properties of hydrothermally prepared CuS nanochips and explored the

✉ Yukti Gupta
yukti_62000006@nitkkr.ac.in; yuktigupta2397@gmail.com

[1] Department of Physics, National Institute of Technology Kurukshetra, Kurukshetra, Haryana 136119, India

[2] Department of Physics, Daulat Ram College, University of Delhi, North Campus, Delhi 110007, India

change in properties with ultrasonically synthesized nanocomposites. They reported that the CNT/CuS nanocomposite showed high conductivity and capacitance compared to CuS nanoparticles.[12]

Among various metal chalcogenides, copper sulfide (CuS) is a non-toxic and non-corrosive material.[13–15] It is a typical *p*-type semiconductor with a direct bandgap width of 1.2–2.0 eV.[16,17] Abhay et al.[18] reported a Cu_xS/FMWCNTs nanocomposite-based sensor that worked at room temperature, which was successfully used to detect NH_3 gas. They showed the variation of the bandgap with the stoichiometry of CuS as the bandgap is considered to be related to the sensitivity of the gas sensor.

In the present work, CuS nanoparticles synthesized via the hydrothermal route were utilized for nanocomposite formation. These nanoparticles were added in FMWCNTs in different wt% using a facile sonication method. The as-synthesized nanocomposites were analyzed for various properties, such as structural, morphological, optical, and electrical, by using different characterization techniques, i.e., X-ray diffraction (XRD) and Raman spectroscopic measurements for structural analysis, field emission scanning electron microscopy (FESEM), energy dispersive X-ray (EDX) for morphological analysis and elemental confirmation, photoluminescence (PL) spectroscopy, UV-Visible spectroscopy for optical measurements, and *I–V* characteristics for electrical analysis. The investigation of the synthesized nanocomposites revealed that the sample can be utilized for gas-sensing applications.

Materials Required for the Synthesis Process

Reagents

Functionalized multiwalled carbon nanotubes (FMWCNTs) procured from Global Nanotech (Mumbai, India) with a purity level of more than 99% were used as a base material to synthesize the nanocomposites. Copper nitrate trihydrate ($Cu(NO_3)_2{\cdot}3H_2O$) supplied by Nice Chemicals and sodium sulfide (Na_2S) supplied by Loba Chemie were used as precursors. De-ionised (DI) water, and ethanol were used as solvents. All the chemicals were used as received without any refinement.

Synthesis of CuS Nanoparticles

A hydrothermal method was employed for the synthesis of CuS nanoparticles. In the preparation process, 0.6 M $Cu(NO_3)_2{\cdot}3H_2O$ and 1.2 M Na_2S were dissolved in two separate beakers in 40 ml DI water each. Both solutions were stirred on a magnetic stirrer for 15 min to prepare uniform solutions. After that, Na_2S solution was added dropwise with the $Cu(NO_3)_2$ solution, then the prepared solution was stirred for 15 min. The final homogeneous solution was transferred to a Teflon crucible in a stainless-steel autoclave and placed in an oven for hydrothermal reaction at 120 °C for 16 h. Next, the precipitates were washed with DI water and ethanol several times, and then dried at 70 °C for 10 h. A substitution reaction took place between the copper nitrate and sodium sulfide in the presence of DI water during the process. In the beaker containing $Cu(NO_3)_2$ solution, copper ions and nitrate ions were formed along with the formation of sodium ions and sulfide ions in the beaker containing Na_2S solution. When these solutions were mixed the copper ions became attached to the sulfide ions and nitrate ions with the sodium ions, resulting in precipitates of CuS, while the other components were removed by the washing.

$$\mathrm{Cu}\left(\mathrm{NO_3}\right)_2 \rightarrow \mathrm{Cu^{2+}} + \left(\mathrm{NO_3}\right)^- \quad \text{(i)}$$

$$\mathrm{Na_2S} \rightarrow \mathrm{Na^+} + \mathrm{S^{2-}} \quad \text{(ii)}$$

$$\mathrm{Cu}\left(\mathrm{NO_3}\right)_2 + \mathrm{Na_2S} \rightarrow \mathrm{CuS}\downarrow + \mathrm{NaNO_3} \quad \text{(iii)}$$

Synthesis of FMWCNTs/ CuS Nanocomposite

The nanocomposites were synthesized by adding CuS nanoparticles in different wt% in carboxyl group functionalized MWCNTs. Initially, 4 wt% of CuS nanoparticles and FMWCNTs were dispersed in different beakers in ethanol via ultrasonication for 15 min. Afterward, the dispersed solution of CuS nanoparticles was added to the FMWCNTs solution dropwise and sonicated again for 30 min. The solution thus obtained was left on the magnetic stirrer for constant stirring of 14 h. The final solution was filtered out, washed with ethanol, to obtain a black residue, and dried at 70 °C. The obtained nanoparticles of FMWCNTs/CuS were labeled as FMWCNT/CuS4%. A similar procedure was followed for 8 wt% and 12 wt% of CuS nanoparticles and the obtained samples were labeled as FMWCNT/CuS8% and FMWCNT/CuS12%, respectively. The synthesis route for the CuS nanoparticles and nanocomposites of FMWCNTs/CuS is shown in Fig. 1.

Characterization Techniques

The XRD patterns of the nanocomposites were recorded on a Rigaku Mini Flex II diffractometer with Cu Kα radiation of wavelength (λ = 1.54 Å), and 20–80° as the scanning angle. Raman spectra were recorded on STR 500 Confocal Raman Spectrometer with laser excitation at 532 nm in the range of 500–3100 cm^{-1}. The morphology was studied using

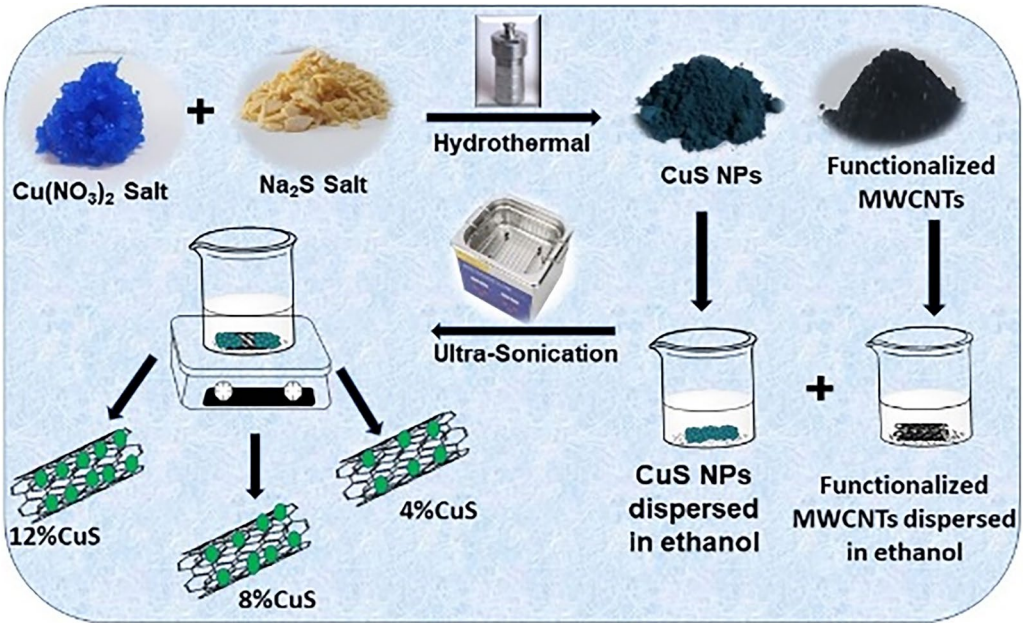

Fig. 1 Schematic of the synthesis route for the preparation of CuS and FMWCNTs/CuS nanocomposites.

field-emission scanning electron microscopy (FESEM) by a Nova Nano FESEM 450, and the existence of the elements was ascertained by energy-dispersive X-ray (EDX) analysis. The photoluminescence (PL) spectra of the nanocomposites were obtained on a Shimadzu RF-5301PC Spectro fluorophotometer, the absorption spectra of the nanocomposites were recorded at room temperature on a Shimadzu UV-3600i Plus UV–Visible Spectrophotometer, and the electrical properties of synthesized samples were optimized using two-probe setups with help of a Keithley 2450 series source meter.

Results and Discussion

Structural Analysis

X-Ray Diffraction Analysis

XRD patterns of the FMWCNTs/CuS nanocomposites are displayed in Fig. 2. The XRD pattern for FMWCNT/CuS4% shows the diffraction peak appearing at 2 = 25.22° and 42.6°, corresponding to characteristic peaks of the (002) and (110) planes of the FMWCNTs, respectively [34]. The diffraction peaks obtained at 29.27°, 31.78°, 32.85°, 47.78°, 52.72°, and 9.34° are indexed as the (102), (103), (006), (107), (108), and (116) planes, respectively, corresponding to ICDD card no. 06-0464, which confirm the formation of the hexagonal phase of covellite CuS nanoparticles. No extra diffraction peaks appeared in the

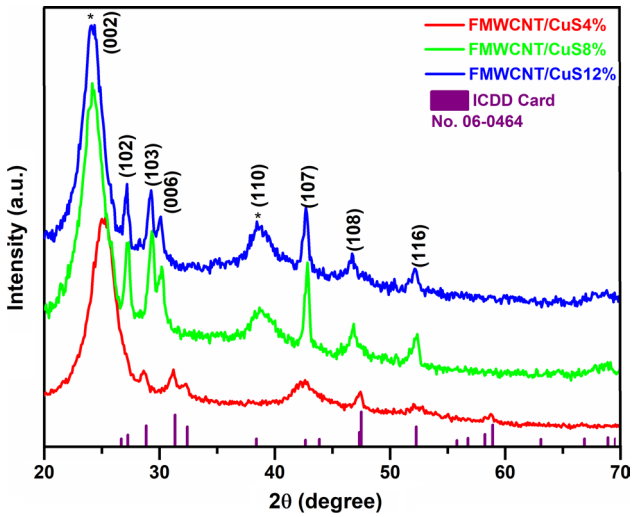

Fig. 2 XRD spectra of the FMWCNTs/CuS4%, FMWCNTs/CuS8%, and FMWCNTs/CuS12% samples.

XRD patterns, revealing that no other impurities were present. The FMWCNT/CuS8% and FMWCNT/CuS12% were prepared by increasing the amount of CuS, and although a similar pattern was obtained for both, the intensity of the XRD peaks gradually increased with the increase in the wt% of the CuS nanoparticles. The crystallinity of FMWCNTs/CuS gradually decreased on increasing the amount of CuS, as the FMWCNTs are more crystalline than CuS nanoparticles; thus, addition of CuS nanoparticles reduces the crystallinity of the nanocomposites.

The crystallite size calculated from the Debye–Scherrer formula[19] as mentioned in Table I. The crystallite size decreased with the addition of CuS. Furthermore, the average d-spacing as calculated by Bragg's law[20] revealed a decrease in the d-spacing between the crystal planes of the CuS, as the value was 2.67 Å for FMWCNT/CuS8% and FMWCNT/CuS12% compared with 2.71 Å for FMWCNT/CuS4%. Equation (1) represents the formula[21] corresponding to the hexagonal structure for calculating the lattice parameters of the CuS nanoparticles, the standard value of lattice parameters being $a = b = 3.79$ and $c = 16.34$ $A°$:

$$\frac{1}{d^2} = \frac{4}{3}\frac{\left(h^2 + hk + k^2\right)}{a^2} + \frac{l^2}{c^2} \tag{1}$$

where θ is the Bragg angle of diffraction, d represents the interplanar distance, (h k l) are Miller indices, and a, b, and c denote the unit cell parameters. The crystallinity of all the samples has been calculated from Eq. (2), as mentioned in Table I:

$$Crystallinity = \frac{Area\ of\ crystalline\ peaks}{Area\ of\ all\ peaks} * 100 \tag{2}$$

The decrease in crystallinity from sample FMWCNT/CuS4% to sample FMWCNT/CuS12%, with the increase in the amount of CuS, might be attributed to the defects induced by the low-crystalline CuS nanoparticles in the FMWCNTs.

Raman Spectroscopy

The Raman spectra of Fthe MWCNT/CuS4%, FMWCNT/CuS8%, and FMWCNT/CuS12% nanocomposites were obtained by exciting the samples at a wavelength of 532 nm using the second harmonic of a solid-state Nd:YAG laser. The spectra shown in Fig. 3 consist of three peaks acquiescent to standard characteristic carbon peaks positioned at 1347 cm^{-1} for the D band, at 1585 cm^{-1} for the G band, and at 2688 cm^{-1} for the 2D band.[22] The D band occurs due to the presence of disorder in the sp^2 structure of the CNTs, and is also related to the sp^3 sites of hexagonal CNTs. The G band is attributed to the graphite Raman active mode and represents the stretching of the C–C bond in sp^2 carbon atoms of CNTs. The crystalline nature of the nanotubes is inversely proportional to the amount of defects. Also, the 2D band is an overtone of the D band which is created due to two-phonon scattering. The Raman spectra have been fitted separately in Fig. 3b, c, and d, confirming the presence of the CuS and C peaks, which are clearly visible.[23] Also, sample FMWCNT/CuS12% has the highest CuS intensity due to the presence of CuS in higher amounts than in the others.

The values of I_D/I_G for FMWCNT/CuS4%, FMWCNT/CuS8%, and FMWCNT/CuS12% were 1.36, 1.7, and 1.98, respectively, which increased monotonously. The I_D/I_G ratio illustrates the degree of defects present in the nanotubes. CuS has introduced structural defects in CNTs that could have changed the ring from hexagonal to pentagonal.[24] The presence of a small peak at 1110 cm^{-1} for the FMWCNT/CuS8% sample increases with a slight shift to 1120 cm^{-1} for the FMWCNT/CuS12% sample, which has the highest amount of CuS. The crystallite size has been calculated by [25]:

$$L_a = \frac{560}{E_L}.\left(\frac{I_D}{I_G}\right)^{-1} \tag{3}$$

where E is the excitation energy of the laser denoted by$_L$, and the crystallite sizes (L_a) were 12.4, 9.92, and 8.52 $A°$ for the FMWCNT/CuS4%, FMWCNT/CuS8%, FMWCNT/CuS12% nanocomposites, respectively

Morphological Analysis

Field-Emission Scanning Electron Microscopy (FESEM) Analysis and Energy-Dispersive X-Ray (EDX) Analysis

FESEM has been used to determine the surface morphology of the nanocomposites. Figure 4 shows the agglomerated CuS nanoparticles with irregular-sized nanoflakes along with the FMWCNTs. The size of the CuS nanoparticles and FMWCNTs were in the range of 35–45 nm and 25–30 nm, respectively, which was determined using imageJ software. It can be concluded from Fig. 4a, b, and c that the presence of CuS nanoparticles increased with the increase in

Table I Comparison of calculated parameters for the structural analysis of FMWCNTs/CuS nanocomposites

Sample no.	Sample name	Crystallite size (D) (nm)	d-spacing (d) ($A°$)	Crystallinity (%)	Lattice parameter (a, b, c) (A°)
1	S1	11.7	2.71	97	a = b = 3.65 c = 17.16
2	S2	9.87	2.67	95	a = b = 3.65 c = 16.66
3	S3	9.01	2.67	94	a = b = 3.65 c = 16.70

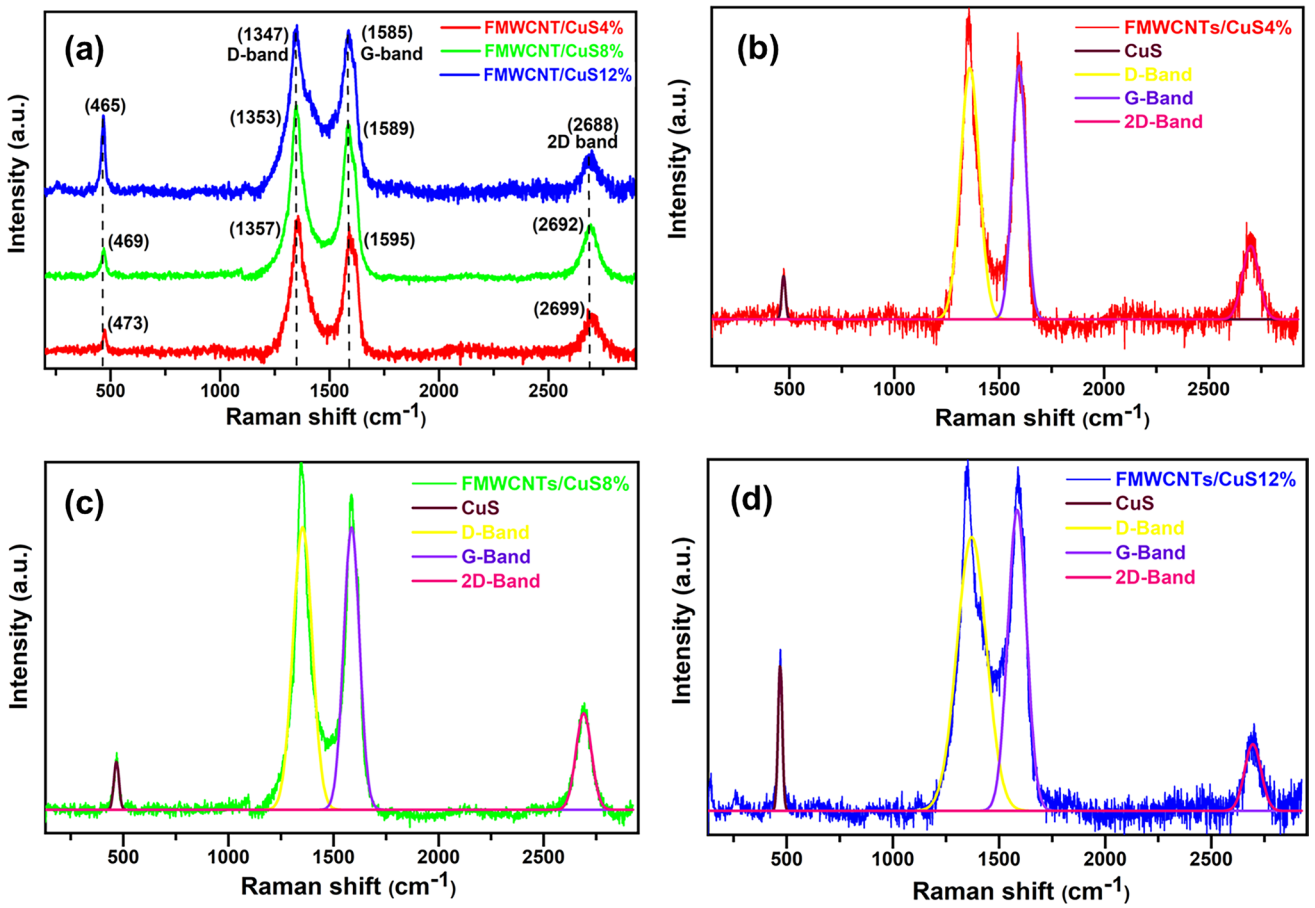

Fig. 3 (a) Comparative Raman spectra of all three samples; fitted Raman spectra of the (b) FMWCNTs/CuS4%, (c) FMWCNTs/CuS8%, and (d) FMWCNTs/CuS12% samples depicting the presence of characteristic peaks for CuS and carbon.

wt% of CuS. The availability of CuS in the nanocomposites of FMWCNTs/CuS, enhanced the charge transfer between energy levels of CuS and FMWCNTs for the generation of a photocurrent.

The chemical composition of the prepared nanocomposite was analyzed using EDX analysis. Figure 4d, e, and f shows that the EDX profiles of the nanocomposites contain the peaks of Cu, S, and C, which confirms the formation of the FMWCNTs/CuS nanocomposites. The elemental % is shown in Table I, which clearly shows the decrease in the concentration of C with the increase in wt% of CuS in the nanocomposites as we go from FMWCNT/CuS4% to FMWCNT/CuS12%.

Optical Properties

UV–Visible Absorption Studies

The UV-Vis absorption spectroscopy facilitates the exploration of the optical properties of the nanocomposites. Figure 5 shows the UV–Vis absorption spectra of the FMWCNT/CuS4%, FMWCNT/CuS8%, and FMWCNT/CuS12% samples plotted in the wavelength range of 280–700 nm. The absorption peaks shown in the spectra are due to the addition of CuS nanoparticles in the FMWCNTs/CuS nanocomposites which exhibit absorption in the UV–Vis region. The absorption peaks are positioned at 297.8, 297, and 295.8 nm for FMWCNT/CuS4%, FMWCNT/CuS8%, and FMWCNT/CuS12%, respectively. Among the three samples, FMWCNT/CuS12% exhibits the highest absorbance.

As is clear from Fig. 5, the light absorption intensity of the UV–Vis spectra decreases monotonously with increasing wavelength, and the spectra are red-shifted with the increase in the amount of CuS nanoparticles.[26]

The Tauc's plot attained from the absorption spectra in Fig. 6 have been used to compute the energy bandgap of the nanocomposites and are given by[27]:

$$\alpha h\upsilon = C\left(h\upsilon - E_g\right)^n \quad (4)$$

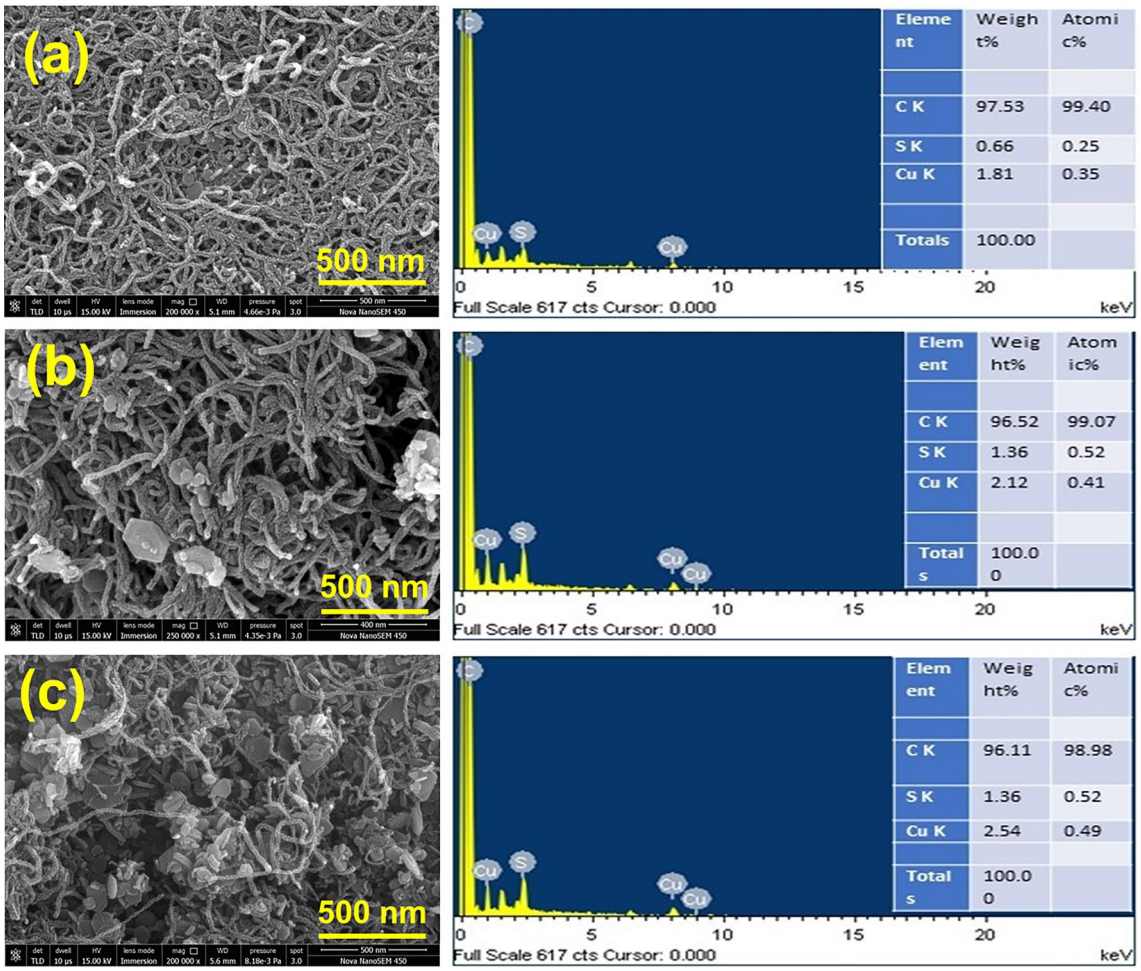

Fig. 4 FESEM image (500 nm) and EDX image of (a) FMWCNTs/CuS4%, (b) FMWCNTs/CuS8%, and (c) FMWCNTs/CuS12% nanocomposites.

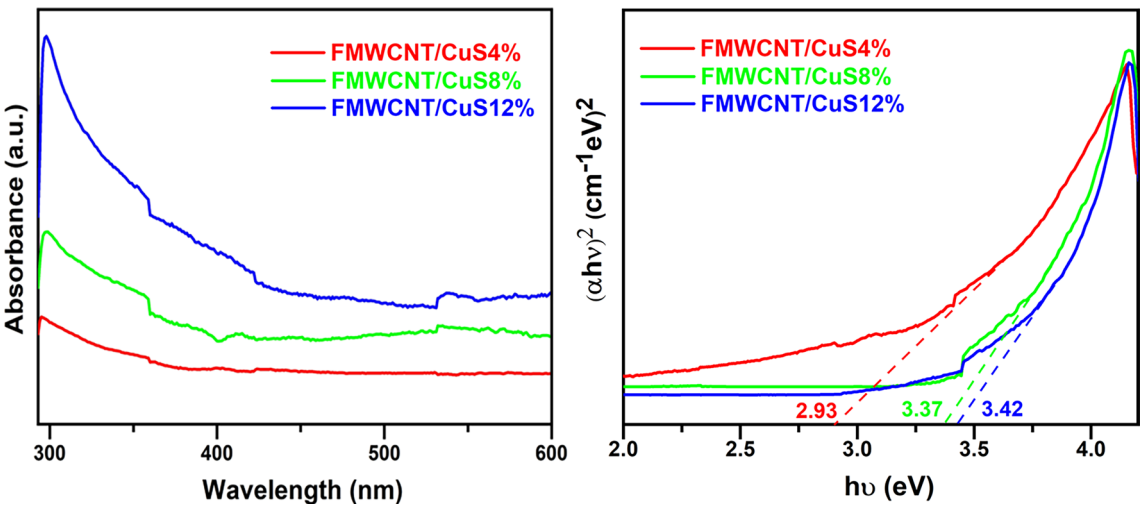

Fig. 5 UV–Vis analysis (*left*) and Tauc's plot (*right*) for FMWCNTs/CuS4%, FMWCNTs/CuS8%, and FMWCNTs/CuS12%.

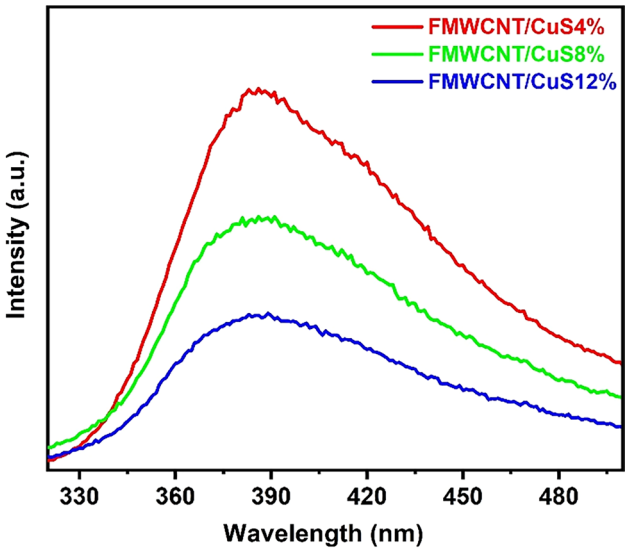

Fig. 6 Photoluminescence spectra of FMWCNTs/CuS4%, FMWCNTs/CuS8%, and FMWCNTs/CuS12% nanocomposites.

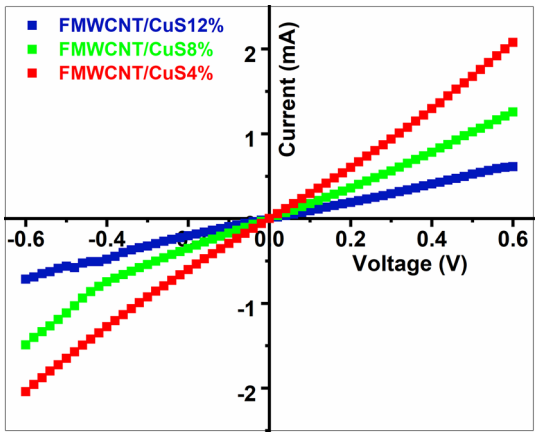

Fig. 7 *I–V* profiles of FMWCNT/CuS nanocomposites.

where α denotes the absorption coefficient, $h\nu$ the photon energy, E_g the optical bandgap in eV, C the energy-dependent constant, and n is the type of transition which can take half-integral values ½ and 3/2 for direct and integral values 2 and 3 for indirect, allowed, or forbidden transitions, respectively. The energy bandgap values were 2.93 for FMWCNT/CuS4%, 3.37 for FMWCNT/CuS8%, and 3.42 eV for FMWCNT/CuS12%.[18] The bandgap of the material is considered to be related to the sensitivity of the gas sensor. The results demonstrate that with an increase in the amount of CuS, the bandgap of the nanocomposite increases, confirming that sample FMWCNT/CuS12% is potential material for sensing applications.

Photoluminescence Spectroscopy

The PL spectroscopy has been used to analyze the electronic states involved in the transfer process of electrons from the excited state to the ground state. Nanotubes, as excellent electrical and thermal conductors, will facilitate the transfer process by causing hindrance in the early recombination of electrons and holes.

The PL spectra of the FMWCNT/CuS4%, FMWCNT/CuS8%, and FMWCNT/CuS12% nanocomposites were obtained at an excitation wavelength of 300 nm, as shown in Fig. 6. When the sample was irradiated with light, the electrons from the valence band became excited and transferred to the conduction band of CuS. As CuS is attached to the FMWCNTs, the electrons become transferred to the conduction band of the FMWCNTs, as they are good acceptors and donors of electrons. Then, the electrons relax and recombine with the holes in the ground state.[28]

The sample FMWCNT/CuS4% shows an emission peak positioned at 386 nm and possesses the highest intensity. With the increase in wt% CuS in the sample, the PL intensity decreased, which could be due to the decrease in the amount of CNTs present in the sample. This led to a reduction in the transfer of electrons from the conduction band of CuS to the conduction band of the CNTs. The nanocomposites FMWCNT/CuS8% and FMWCNT/CuS12% show emission peaks at 387 and 389 nm, respectively, and the peak positions are red-shifted by 2 nm. The decreased PL intensity facilitates easy charge separation and prolonged lifetimes of the excited charge carriers in the nanocomposites. This shows that sample FMWCNT/CuS12% should have improved photovoltaic characteristics.

Electrical Analysis

The current–voltage (*I–V*) measurements of the FMWCNTs/CuS nanocomposites was conducted to measure their conductance. To study the conductance of the samples, they were compressed into uniform-sized pellets. The ohmic behavior for the samples ares shown in Fig. 7. For sample FMWCNT/CuS4%, the value of the current was 1.3 mA. As discussed earlier, the FMWCNTs are good acceptors and donors of electrons, thus making them highly conducting. CuS being a semiconductor acquires less conductivity relative to the FMWCNTs.[29] Furthermore, the increased amount of CuS in the FMWCNTs brings down the conductivity, hence decreasing the value of current. As the amount of CuS in the nanocomposites increases, this causes a decrease in the value of the current. which for FMWCNT/CUS8% and FMWCNT/CUS12% was 0.76 mA and 0.39 mA, respectively.

The variation of conductivity in the nanocomposites with respect to each other is shown in Fig. 8, clearly demonstrating that sample FMWCNT/CuS4% exhibits the highest

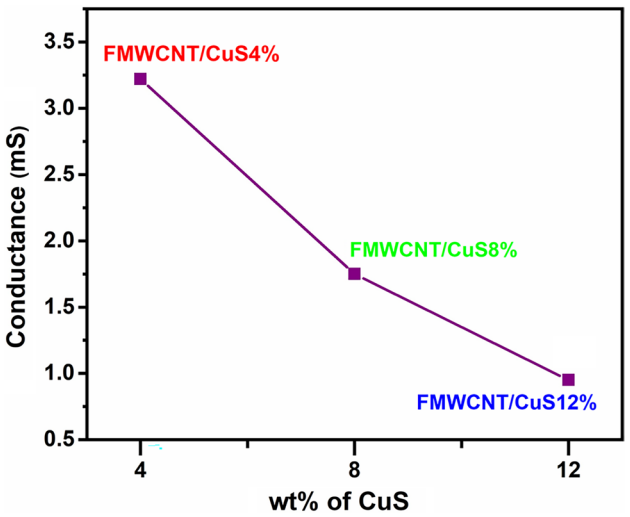

Fig. 8 Variation in conductance values with the increase in wt% of CuS in the samples FMWCNTs/CuS4%, FMWCNTs/CuS8%, and FMWCNTs/CuS12%.

conductance value of 3.22 mS, then sample FMWCNT/CuS8% with 1.75 mS, which is higher than sample FMWCNT/CuS12% (0.95 mS).

Conclusions

FMWCNTs/CuS nanocomposites were prepared via a facile sonication technique, using carboxyl group functionalized MWCNTs and hydrothermally synthesized copper sulfide (CuS) nanoparticles. The effect of the increase in wt% of CuS nanoparticles in the nanocomposites is reported. The analysis of Raman spectra confirmed the presence of characteristic bands of carbon, positioned at 1347 cm^{-1}, 1588 cm^{-1}, and 2692 cm^{-1} for the D band, G band, and 2D band, respectively and 470 cm^{-1} for CuS. The XRD measurements exhibited peaks of the hexagonal covellite phase of CuS. FESEM analysis revealed that the structure of the FMWCNTs was intact and that nanoflake-like CuS was attached to the CNTs. Furthermore, EDX analysis confirmed the presence of Cu, S, and C, along with a decrease in the amount of C with an increase in Cu and S. The PL studies established the application of the nanocomposites in gas sensing by showing easy charge separation and longer lifetimes, which make the material active for a longer time, leading to adsorption of gas molecules. The result of the UV-Visible study shows an increase in the bandgap of the samples with an increase in wt% of CuS, which demonstrates the increase in sensitivity of the sample. The *I–V* characteristics show that the nanocomposites are conducting. Based on the above analysis, sample FMWCNT/CuS4% could be a potential candidate for photo-resistive sensors, while sample FMWCNT/CuS12% could be a potential material for gas-sensing applications.

Acknowledgments Author Yukti Gupta and Mayank Mittal are thankful to Director, National Institute of Technology, Kurukshetra for providing the Fellowship. The author gratefully acknowledges to Dr. Ashish Gupta, Department of Physics, National Institute of Technology, Kurukshetra. The author is also grateful to MNIT, Jaipur, for providing the facility of FESEM and Raman characterizations. The author also acknowledges Dr. Sanjeev Aggarwal, Director Ion Beam Centre, Kurukshetra University, Kurukshetra for providing UV-Visible spectroscopy facility.

Author contributions Yukti Gupta and Mayank Mittal contributed equally to this work

Competing interest The authors declare that they have no known competing financial interests or personal relationships that could have appeared to influence the work reported in this paper.

References

1. Q. Liu, S. Zhang, and Y. Xu, Two-Step Synthesis Nanocomposite as Advanced Electrode Materials for Supercapacitor Applications. *Nanomaterials* 10, 1034 (2020).
2. N. Karikalan, R. Karthik, S.M. Chen, C. Karuppiah, and A. Elangovan, Sonochemical Synthesis of Sulfur Doped Reduced Graphene Oxide Supported CuS Nanoparticles for the Non-enzymatic Glucose Sensor Applications. *Sci. Rep.* 7, 2494 (2017).
3. L. Zhu, M. Gao, C.K.N. Peh, and G.W. Ho, Solar-Driven Photothermal Nanostructured Materials Designs and Prerequisites for Evaporation and Catalysis Applications. *Mater. Horizons* 5, 323 (2018).
4. J. Zhang, H. Shen, Y. Xu, B. Xu, Y. Feng, J. Ge, and Y. Li, Excellent Near-Infrared Response Performance in p-CuS/n-Si Heterojunction Using a Low-Temperature Solution Method. *Surf. Interfaces* 26, 101430 (2021).
5. M. Li, W. Ren, R. Wu, and M. Zhang, CeO_2 Enhanced Ethanol Sensing Performance in a CdS Gas Sensor. *Sensors (Switzerland)* 17, 1 (2017).
6. Q. Chen, S.Y. Ma, X.L. Xu, H.Y. Jiao, G.H. Zhang, L.W. Liu, P.Y. Wang, D.J. Gengzang, and H.H. Yao, Optimization Ethanol Detection Performance Manifested by Gas Sensor Based on In_2O_3/ZnS Rough Microspheres. *Sens. Actuators B Chem.* 264, 263 (2018).
7. J. Li, M. Liu, J. Jiang, B. Liu, H. Tong, Z. Xu, C. Yang, and D. Qian, Morphology-Controlled Electrochemical Sensing Properties of CuS Crystals for Tartrazine and Sunset Yellow. *Sens. Actuators B Chem.* 288, 552 (2019).
8. G. Goswami, A. Mukherjee, A.K. Das, R. Ghosh, and A.K. Meikap, Synthesis, Characterization and Electrical Property of MWCNT-ZnS Nanocomposite Embedded in Polyaniline. *Adv. Nat. Sci. Nanosci. Nanotechnol.* 8, 025018 (2017).
9. R. Sahu, S.K. Jain, and B. Tripathi, A Comparative Study on Visible Light Induced Photocatalytic Activity of MWCNTs Decorated Sulfide Based (ZnS & CdS) Nano Photocatalysts. *Adv. Mater. Nano Syst. Theory Exp.* 2, 179 (2022).
10. M.F. Abou Taleb, N. Shaheen, F.I.A. El Fadl, H.A. Albalwi, M.M. Ibrahim, and M.F. Warsi, Synthesis of CuS/CNTs/GCN Ternary Nanocomposite for Enhanced Photocatalytic Response of Harmful Organic Effulents. *J. Alloys Compd.* 958, 170468 (2023).
11. Y. Zhang, J. Tian, H. Li, L. Wang, X. Qin, A.M. Asiri, A.O. Al-Youbi, and X. Sun, Biomolecule-Assisted, Environmentally

Friendly, One-Pot Synthesis of CuS/Reduced Graphene Oxide Nanocomposites with Enhanced Photocatalytic Performance. *Langmuir* 28, 12893 (2012).
12. H. Sabeeh, M. Aadil, S. Zulfiqar, A. Rasheed, N.F. Al-Khalli, P.O. Agboola, S. Haider, M.F. Warsi, and I. Shakir, Hydrothermal Synthesis of CuS Nanochips and Their Nanohybrids with CNTs for Electrochemical Energy Storage Applications. *Ceram. Int.* 47, 13613 (2021).
13. M. Darouie, S. Afshar, K. Zare, and M. Monajjemi, Investigation of Different Factors towards Synthesis of CuS Spherical Nanoparticles. *J. Exp. Nanosci.* 8, 451 (2013).
14. M.P. Motaung, D.C. Onwudiwe, L. Wei, and C. Lou, CuS, In2S3 and CuInS2 Nanoparticles by Microwave-Assisted Solvothermal Route and Their Electrochemical Studies. *J. Phys. Chem. Solids* 160, 110319 (2022).
15. K. Vinotha, B. Jayasutha, M.J. Abel, and K. Vinoth, In_{3+}-Doped CuS Thin Films: Physicochemical Characteristics and Photocatalytic Property. *J. Mater. Sci. Mater. Electron.* 33, 22862 (2022).
16. Y. Gupte and N. Jaggi, Integrated Hydrothermal-green Synthesis Approach for Covellite CuS Nanoparticles with Enhanced Energy Bandgap for BLEDs. *Mater. Electron.* 30, 34 (2023).
17. V. Bhatt, M. Kumar, and J.-H. Yun, Unraveling the Photoconduction Characteristics of Single-Step Synthesized CuS and Cu9S5 Micro-Flowers. *J. Alloys Compd.* 891, 161940 (2022).
18. A.A. Sagade and R. Sharma, Copper Sulphide (CuxS) as an Ammonia Gas Sensor Working at Room Temperature. *Sens. Actuators B Chem.* 133, 135 (2008).
19. M. Mousavi-Kamazani, Z. Zarghami, and M. Salavati-Niasari, Facile and Novel Chemical Synthesis, Characterization, and Formation Mechanism of Copper Sulfide (Cu2S, Cu2S/CuS, CuS) Nanostructures for Increasing the Efficiency of Solar Cells. *J. Phys. Chem. C* 120, 2096 (2016).
20. A.R. Stokes and A.J.C. Wilson, The Diffraction of X Rays by Distorted Crystal Aggregates - I. *Proc. Phys. Soc.* 56, 174 (1944).
21. P. Bindu and S. Thomas, Estimation of Lattice Strain in ZnO Nanoparticles: X-Ray Peak Profile Analysis. *J. Theor. Appl. Phys.* 8, 123 (2014).
22. T. Ahamad, M. Naushad, and S.M. Alshheri, Fabrication of Highly Porous N/S Doped Carbon Embedded with CuO/CuS Nanoparticles for NH_3 Gas Sensing. *Mater. Lett.* 268, 127515 (2020).
23. V. Bhatt, M. Kumar, E.-C. Kim, H.J. Chung, and J.-H. Yun, Temperature-Dependent Phase Formation of CuInSe2 for Self-Biased, Broadband Si/$CuInSe_2$ Heterojunction Photodetector. *J. Alloys Compd.* 922, 166190 (2022).
24. A. Gupta, S.R. Dhakate, P. Pal, A. Dey, P.K. Iyer, and D.K. Singh, Diamond and Related Materials EFfect of Graphitization Temperature on Structure and Electrical Conductivity of Poly-Acrylonitrile Based Carbon Fi Bers. *Diam. Relat. Mater.* 78, 31 (2017).
25. L.G. Caṇado, K. Takai, T. Enoki, M. Endo, Y.A. Kim, H. Mizusaki, A. Jorio, L.N. Coelho, R. Magalhães-Paniago, and M.A. Pimenta, General Equation for the Determination of the Crystallite Size La of Nanographite by Raman Spectroscopy. *Appl. Phys. Lett.* 88, 163 (2006).
26. N. Jaggi, Effect of Reaction Temperature on Structural and Optical Properties of CuS Nanoparticles. *Indian J. Eng. Mater. Sci.* 30, 447 (2023).
27. S. Noor, S. Sajjad, S.A.K. Leghari, S. Shaheen, and A. Iqbal, ZnO/TiO_2 Nanocomposite Photoanode as an Effective UV-Vis Responsive Dye Sensitized Solar Cell. *Mater. Res. Express* 5, 95905 (2018).
28. A. Gupta, N. Khosla, V. Govindasamy, A. Saini, K. Annapurna, and S.R. Dhakate, Trimetallic Composite Nanofibers for Antibacterial and Photocatalytic Dye Degradation of Mixed Dye Water. *Appl. Nanosci.* 10, 4191 (2020).
29. B.P. Singh, D. Singh, R.B. Mathur, and T.L. Dhami, Influence of Surface Modified MWCNTs on the Mechanical, Electrical and Thermal Properties of Polyimide Nanocomposites. *Nanoscale Res. Lett.* 3, 444 (2008).